AIP | Physics of Plasmas
#1 JOURNAL IN 2014 GOOGLE SCHOLAR METRICS FOR THE PLASMA & FUSION CATEGORY

The development and interaction of instabilities in intense relativistic electron beams

S. A. Kurkin, A. A. Badarin, A. A. Koronovskii, and A. E. Hramov

Citation: Physics of Plasmas **22**, 122110 (2015); doi: 10.1063/1.4938216
View online: http://dx.doi.org/10.1063/1.4938216
View Table of Contents: http://scitation.aip.org/content/aip/journal/pop/22/12?ver=pdfcov
Published by the AIP Publishing

PHYSICS OF PLASMAS **22**, 122110 (2015)

The development and interaction of instabilities in intense relativistic electron beams

S. A. Kurkin,[a)] A. A. Badarin, A. A. Koronovskii, and A. E. Hramov
Saratov State Technical University, Politechnicheskaja 77, Saratov 410054, Russia and Saratov State University, Astrakhanskaja 83, Saratov 410012, Russia

(Received 13 August 2015; accepted 7 December 2015; published online 24 December 2015)

We report on the physical mechanisms of development, coexistence and interaction of Pierce-Bursian and diocotron instabilities in the non-neutral relativistic electron beam (REB) in the classic vircator. The analytical and numerical analysis is provided by means of 3D electromagnetic simulation. We conducted an extensive study of characteristic regimes of REB dynamics determined by the instabilities development. As a result, a regime map has been obtained. It demonstrates sequential switching of the REB dynamics from the regime with $N = 1$ to the regime with $N = 7$ electron bunches in the azimuth direction with the beam current growth for the different external magnetic fields. The numerical analysis of bunch equilibrium states has identified the physical causes responsible for the REB regime switchings.
[http://dx.doi.org/10.1063/1.4938216]

I. INTRODUCTION

Relativistic electron beams (REBs) have a great significance for the modern plasma physics and high-power microwave (HPM) and terahertz (THz) vacuum and plasma electronics due to their wide spectrum of applications in the different areas, such as plasma heating, inertial fusion, high-power microwave generation, etc.[1–4] Intense REBs are known to demonstrate the complex regimes of dynamics including the development of the different types of instabilities, such as Pierce, Bursian, current-convective, slipping, diocotron, Weibel instabilities, etc.[5–10] On the one hand, development of some of these instabilities may play a positive role. For instance, Pierce and Bursian instabilities lead to the formation of the nonstationary virtual cathode (VC) in the electron beam with the overcritical current.[1,11–15] This effect is used in a perspective class of microwave devices called virtual cathode oscillators (or vircators) that belong to a special class of bremsstrahlung microwave generators and amplifiers.[11–14,16–18] On the other hand, instabilities in the REBs may have a negative impact on the operation of high-power microwave and THz devices, accelerators, plasma heating and inertial fusion systems, etc., and impose certain limitations on the regimes of their operation.[5–7,9] For example, the development of the aforementioned Pierce or Bursian instabilities limits the maximal current that may be transported through an equipotential drift space.[19–22] Diocotron and slipping instabilities influence considerably the intense beam geometry during its propagation through a system. It leads to the development of the azimuthal and radial nonuniformities in the REB, particularly, to the formation of vortex and spiral structures and to the filamentation of the beam.[23–33] These effects are often undesirable for the operation of systems using beams of charged particles. The diocotron and slipping instabilities usually occur in HPM devices, beam collimator systems in high-energy colliders (such as the Tevatron or the Large Hadron Collider in CERN), Penning traps, etc. Therefore, mitigation or control of these instabilities is an important problem for the development of HPM, inertial fusion, accelerator, collider, and other systems. In this case, the intense high-energy beams of charged particles are used on relatively long distances or for long times (like in the beam traps).[8,33–36] Different methods for mitigation or control of such instabilities are actively studied at present.[34,37,38] At the same time, the diocotron and slipping instabilities could be useful for the development of novel methods for HPM generation (see, for example, the work[23] where the effect of the microwave generation from the filamentation and vortex formation within magnetically confined electron beams was discovered and investigated).

It should be noted that the conditions for the simultaneous development of several instabilities often arise in the intense beams of charged particles.[39–41] The typical situation is the coexistence of Bursian/Pierce and diocotron (slipping) instabilities in REB. Such complex regimes of the beam dynamics have been poorly investigated so far though their study is important both for fundamental and applied purposes. It is all the more important due to the development of HPM and THz electronics sources, especially for the optimization of relativistic vircators, where Bursian/Pierce and diocotron (slipping) instabilities often coexist and it influences considerably the generation characteristics of the device.[39,40,42] Nowadays, a rising interest in the research of vircators is caused by their advantages: a very high output microwave radiation power, a simple construction (in particular, vircators can operate without external focusing magnetic field), short rise time, the possibility of a simple frequency tuning and regime switching (tunability), a rather short operation region, and low requirements to the quality of the electron beam.[1,14,15,43–50] The last property is of great importance when an oscillator is fed with a short and low-quality beam formed by an explosion emission electron injector.[51,52]

[a)]Electronic mail: KurkinSA@gmail.com

So, the subject of the present work is determined by the above-named problems and devoted to the detailed investigation of the physical mechanisms of the coexistence, joint development, and interaction of Bursian and diocotron instabilities in the nonneutral REB in the classic relativistic vircator model. The structure of the paper is as follows. In Section II, we briefly describe the proposed numerical model. In Section III, the physical processes occurring during the joint development of the instabilities are considered and analyzed. In Section IV, the characteristic regimes of REB dynamics determined by the development of instabilities are investigated in detail. In Section V, we reveal analytically and numerically the physical background for the REB regime switchings.

II. SYSTEM UNDER STUDY

In analyzing REBs, it is necessary to take into account effects which are insignificant for the weakly relativistic systems, specifically the influence of the self-magnetic field of a REB.[40,42] The simultaneous coexistence of two instabilities in a REB leads to the complex beam dynamics in the system that may be efficiently analyzed mainly with the help of the numerical methods based on the solving the self-consistent system of Maxwell equations and motion equations of charged particles. For this reason, the 3D fully electromagnetic particle-in-cell (PIC) solver of CST Particle Studio package is used in our work for the accurate numerical investigations of REB dynamics in the relativistic vircator model.

The system under study (see Fig. 1(a)) consists of a perfect electric conducting finite–length cylindrical equipotential waveguide region *1* (an electron beam drift chamber) of the length L, the radius R, with an entrance transparent grid electrode 2 on the left side and an output coaxial waveguide port 3 on the right side.[40,53] An axially symmetrical monoenergetic annular relativistic electron beam 4 with the current I_0, the initial electron energy W_e (850 keV in this work), the external radius R_b, and the thickness d is injected through the entrance electrode 2. Electrons can leave the waveguide region by reaching the side wall or the right (collector) end of the drift chamber 5.

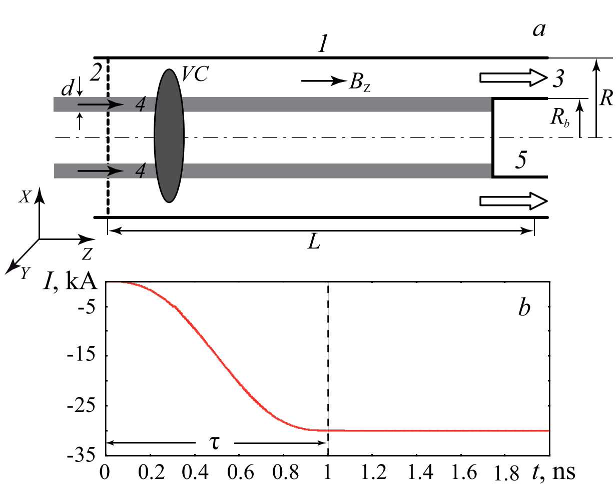

FIG. 1. (a) The scheme of the investigated system in section. Here, *1* is a cylindrical equipotential drift chamber, *2*—an entrance transparent grid electrode (an injection plane), *3*—an output coaxial waveguide port, *4*—an axially symmetrical monoenergetic annular relativistic electron beam, and *5*—a cylindrical collector. *B* is the external uniform focusing magnetic field; VC denotes schematically the virtual cathode area. (b) The shape of the current pulse (only a part of the pulse is shown in the figure); the full duration of the pulse is 100 ns; and the time step Δt used in the calculations is 1.93×10^{-4} ns.

In the present study, the values of geometric parameters were chosen as: $L = 45$ mm, $R = 10$ mm, $R_b = 5$ mm, and $d = 1.5$ mm. Also note that the waveguide is superdimensional in the respect of a wavelength corresponding to a vircator fundamental generation frequency. The external uniform magnetic field with induction $B_z = B_0 \in (0, 2)$ T is applied along the longitudinal (z) axis of the waveguide. We suppose that the injected REB is formed by a magnetically insulated diode.[54] The beam current pulse has the smooth step shape (see Fig. 1(b)) with the rise time of 1 ns and the full duration of 100 ns. The time step used in the calculations is $\Delta t = 1.93 \times 10^{-4}$ ns, and the consequent error is estimated as $O(\Delta t)$.

III. PHYSICAL MECHANISMS OF THE INSTABILITIES DEVELOPMENT

The diocotron instability is the shear instability that is driven by shear in the drift velocity of charged particles perpendicular to the magnetic field, and it leads to the filamentation of a beam and often to the vortex formation.[36,55–58] This instability is observed in many plasma systems including planetary atmospheres, pulsar magnetospheres, aurora borealis, beams of charged particles, etc.[57,59]

The Bursian instability[19,60–62] appears in the beam of the charged particles travelling through a drift space due to an uncompensated space charge leading to the sagging of potential in the system. The main condition for the Bursian instability development in the electron beam is that the beam current should be greater than the critical value (the so-called space-charge-limited (SCL) or Bogdankevich–Rukhadze current).[21,22] In this case, the dense cloud of decelerated electrons (electron bunch, corresponding to virtual cathode) is formed in the area of the potential sagging. A virtual cathode reflects a part of electrons back to the entrance plane or on the side wall of the drift tube and is characterized usually by the complex non-stationary dynamics.[15,39,40,42,63–68]

The conditions for the development of two above-mentioned instabilities are often satisfied in the considered system with intense REB. Let us consider the physical processes occurring in the REB during the instabilities development, analyzing the dependencies of the radius-averaged space charge density $\rho(\varphi)$ and the azimuthal velocity $v_\varphi(\varphi)$ of the REB and space charge density distributions in the system $\rho(x, y)$ for the character system parameters ($I_0 = 40$ kA and $B_0 = 0$ T). The chosen parameters correspond to the case of the joint development of the diocotron and Bursian instabilities (see Fig. 2). The listed characteristics allow to analyze effectively the processes of electron structures formation in the system. The longitudinal coordinate z_s of the cutting plane, where the space charge density distributions were obtained, corresponds approximately to the mean virtual cathode position and equals to 2 mm.

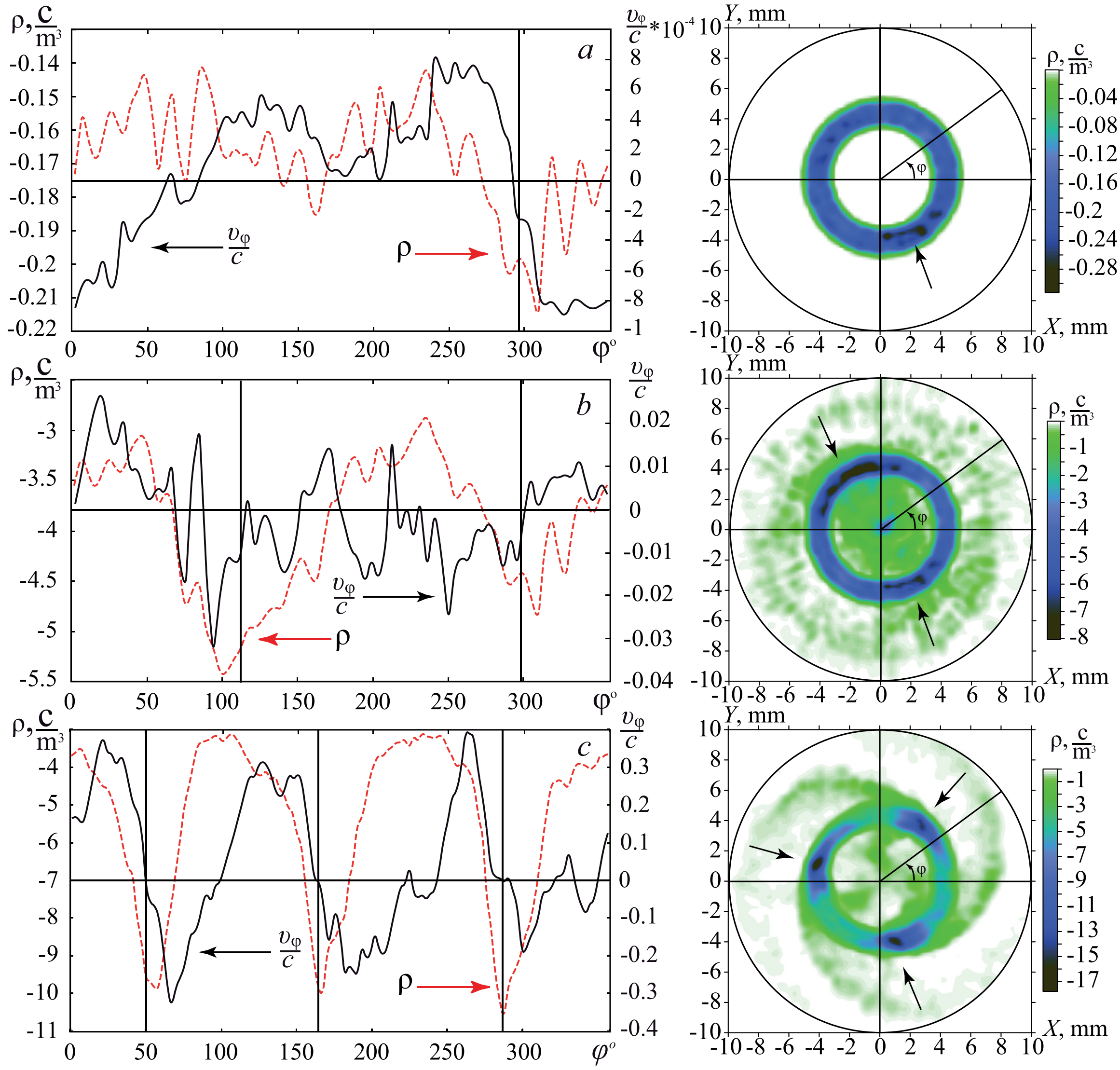

FIG. 2. The dependencies of the radius-averaged space charge density $\rho(\varphi)$ (dashed curves) and the azimuthal velocity $v_\varphi(\varphi)$ (solid curves) of the REB on the azimuthal coordinate φ (left figures) and space charge density distributions in the system $\rho(x, y)$ (right figures) at the cross-section (x, y) at the following character instants of time t: $t = 0.2$ ns (*a*), $t = 0.73$ ns (*b*), and $t = 51$ ns (*c*) for the beam current $I_0 = 40$ kA without an external magnetic field ($B_0 = 0$); the longitudinal coordinate of the cutting plane $z_s = 2$ mm that corresponds approximately to the mean virtual cathode position. The vertical lines in left figures and the arrows in right figures denote the centers of the electron bunches.

So, at the beginning of the REB propagation (Fig. 2(a), $t = 0.2$ ns), one electron bunch is formed in the azimuthal direction, the maximum (in absolute value) on the dependency $\rho(\varphi)$, and the dark area on the space charge density distribution correspond to this bunch. It is the initial stage of the diocotron instability development that arises due to the presence of the velocity gradient (shear) $\partial v_\varphi / \partial \varphi \neq 0$: the bunch starts forming in the area where the azimuthal velocity changes its sign from positive to negative, and two different parts of the beam move opposite to each other (see Fig. 2(a)). It should be noted that values of the azimuthal velocity and space charge density are small at this initial stage.

The Bursian instability is developed in parallel to the diocotron instability because the beam current exceeds the critical value $I_{SCL} \approx 8$ kA considerably. The consequence is the rise of the space charge density and, as a result, formation of the virtual cathode, approximately in the area of the cutting plane position in Fig. 2. So, Fig. 2(b) ($t = 0.73$ ns) demonstrates the case when the virtual cathode appears (starts) in the system that leads to the reflections of electrons from it (the reflected electrons form the halo around the annular REB on the space charge density distribution in Fig. 2(b)). The space charge density increases in the system as a result of the Bursian instability development and the beam current growth. (It should be remembered that the rise time of the current pulse is 1 ns.) Additionally, the second bunch is formed in the azimuthal direction.

Finally, Fig. 2(c) ($t = 51$ ns) shows the steady-state REB structure after the long transient process determined by the instabilities development and interaction. It is characterized by the presence of three electron bunches rotating in the azimuthal direction. In fact, these bunches are the VC with the complex configuration in the azimuthal direction, and electrons are mainly reflected from them. The rotation of the bunches is determined by their destruction because of the electrons reflections and the formation of a new bunch in azimuth near the destructed one. In other words, the space-charge wave (the disturbance wave) is excited in the azimuthal direction because of the interaction of the instabilities: the diocotron instability leads to the REB filamentation and the Bursian—to electron reflections and further bunches rotation. It is important to note that the Bursian instability contributes to the development of the diocotron instability, since it considerably increases the space charge density in the area near the injection plane and, as a consequence, the increment of the diocotron instability development due to the growth of the velocity gradient.[23,26,31,33,57]

Let us consider physical causes responsible for the diocotron instability development in the investigated system. The presence of external magnetic field as a consequence of the excitation of the electrodynamic system eigenfields by the intense high-energy REB is not a necessary condition for the instability origin in the system with a REB (see, for example, the case shown in Fig. 2). In contrast, the most significant for the diocotron instability development is the longitudinal component of the sum of induced magnetic and REB self-magnetic fields in the system; distributions of that are shown in Fig. 3. Fig. 3(a) corresponds to the very beginning of the REB front propagation in the drift chamber ($t = 0.005$ ns) and is characterized by a number of the local magnetic microfields generated by the radial microcurrents created by the separate local groups of electrons.

At the same time, the REB front excites a low amplitude wide spectrum of the electrodynamic system eigenmodes at the beginning of the current pulse. One of the eigenmodes that coincides better with the REB self-fields and has a frequency close to the character beam frequency (plasma frequency that depends on the beam current and lies in the range 15–50 GHz in the present study) increases over time. Particularly, such an effect is expressed in Fig. 3 in the formation of the definite magnetic field configuration according to the eigenmode one, and Fig. 3(b) corresponds to the transitional moment $t = 0.015$ ns when separate microfields are merging, approaching to the developed eigenmode's magnetic field structure that is shown in Fig. 3(c) for $t = 0.15$ ns. Let us emphasize that the Bursian instability exactly contributes to the excitation of the character eigenmode in the system due to the establishing of the typical intense electric self-field distribution with the potential sagging.

The typical form of the induced eigenmode longitudinal magnetic field, characterized by different signs (see Fig. 3(c)), causes parts of the REB to move opposite to each other in the azimuthal direction ($\partial v_\varphi / \partial \varphi \neq 0$). As a result, the electron bunches arise in the areas where H_z changes a sign from minus to plus (when moving clockwise in the azimuthal direction)—the filamentation of the REB occurs. Notice that the relatively weak eigenmode longitudinal magnetic field plays a significant role only at the initial stage of the instabilities development that ends approximately at $t \approx 0.1 - 0.3$ ns when the REB magnetic self-field H_z takes the similar configuration as that of the induced eigenmode. Further beam dynamics is mainly determined by the self-consistent REB fields.

IV. REGIMES OF THE UNSTABLE REB DYNAMICS

As has been stated above, the electron bunches are formed in the relativistic electron beam of the considered system due to the joint development of the diocotron and Bursian instabilities. Various regimes with the different number of bunches are established in the system after the transient process depending, particularly, on the beam

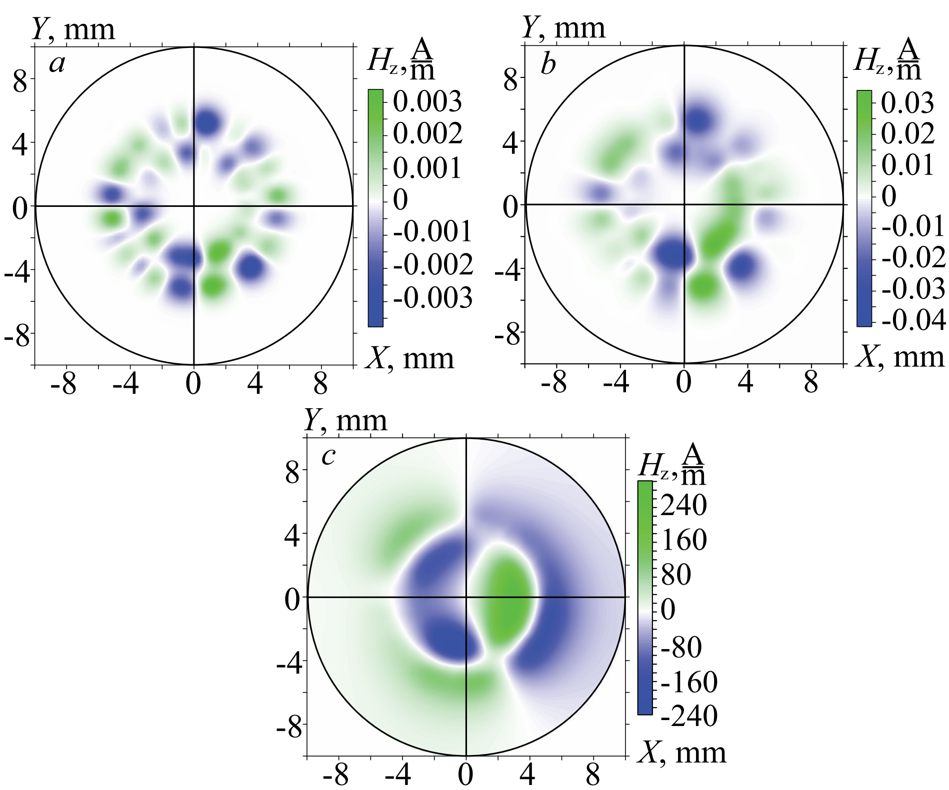

FIG. 3. The distributions of the longitudinal component of the sum of induced magnetic and REB self-magnetic fields in the system $H_z(x, y)$ at the cross-section (x, y) at the following character instants of time t: $t = 0.005$ ns (a), $t = 0.015$ ns (b), and $t = 0.15$ ns (c) for the beam current $I_0 = 40$ kA without the external magnetic field ($B_0 = 0$); the longitudinal coordinate of the cutting plane $z_s = 2$ mm that corresponds approximately to the mean virtual cathode position.

current and the external magnetic field values. For the detailed analysis of the unstable REB dynamics regimes with control parameters' variations, the regime map in the plane (I_0, B_0) has been obtained (Fig. 4). The induction of external magnetic field and the beam current was changed in the calculations with the steps 0.05 T and 1 kA, respectively.

Fig. 4 demonstrates regimes with $N = 1 - 7$ electron bunches in the azimuthal direction for the overcritical values of the beam current when both considered instabilities are developed. The basic tendency here is that with the beam current growth we observe the sequential switching of the REB dynamics from the regime with $N = 1$ to the regime with $N = 7$ bunches for the different external magnetic fields, and this tendency is more clearly defined for the relatively strong external magnetic fields $B > 1.5$ T. The regimes with the odd numbers of the bunches N are characterized by the narrower regions in comparison with the regimes with even N, and these regions are often embedded in the regions with even N in the form of the so-called "narrow windows."

The typical configuration portraits of the REB at the transverse plane are presented in Fig. 5 for six character sets of parameters of the unstable beam dynamics. One can see that the value of the external magnetic field influences the REB configuration considerably. If it is relatively low and the defocusing forces are greater than the magnetic focusing ones, then the formed electron bunches give rise to the rotating vortex structures (see Figs. 5(a)–5(d)) due to the simultaneous action of the defocusing forces and rotation of the REB. Otherwise, in the case of the strong external magnetic field the electron bunches appear magnetized and do not exceed the external beam radius essentially (see Figs. 5(e) and 5(f) obtained for $B_0 = 20$ kG). Note also that the formed electron bunches have the spiral form along the longitudinal direction (z-axis, see Fig. 5(g)) up to the area of their destruction because of the virtual cathode formation or the action of the defocusing forces. So, the spiral structure is better developed for the cases of low beam currents and strong

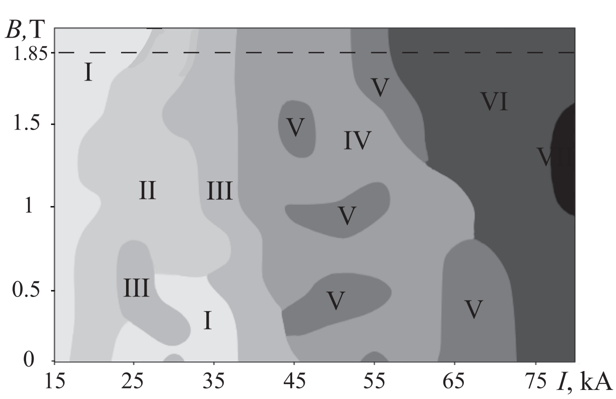

FIG. 4. The typical REB dynamics regimes in the considered system in the "beam current I_0–external magnetic field B_0" plane. Roman numerals denote the regions with the different regimes of REB dynamics, and the value of the numeral N corresponds to the regime with N electron bunches in the azimuthal direction; the dotted line refers to the results presented in Fig. 7. The grid of the parameters' plane used for the calculation of the regime map has 1 kA step in the beam current and 0.05 T step in the magnetic field induction.

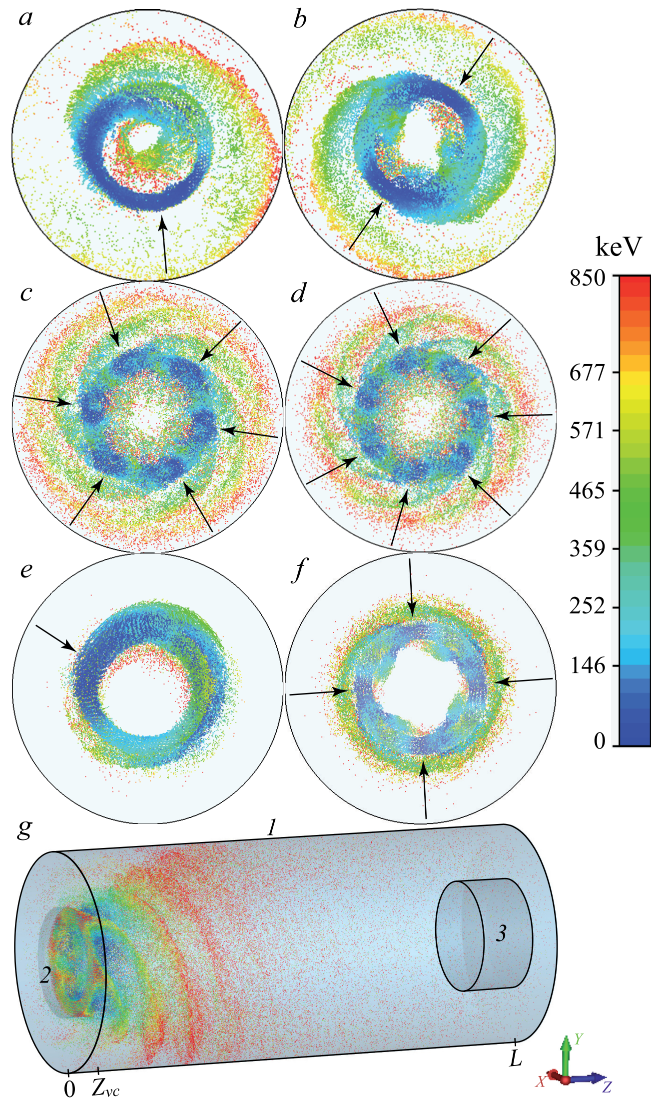

FIG. 5. Projections of the instantaneous positions of the electron beam charged particles (configuration portraits) at the cross-section (x, y) for $I_0 =$ 30 kA, $B_0 = 4$ kG (*a*, the regime with $N = 1$ electron bunches, the VC position relative to the injection plane $z_{VC} = 1.45$ mm), $I_0 = 30$ kA, $B_0 = 6$ kG (*b*, $N = 2$, $z_{VC} = 1.2$ mm), $I_0 = 80$ kA, $B_0 = 14$ kG (*c*, $N = 6$, $z_{VC} = 0.48$ mm), $I_0 = 75$ kA, $B_0 = 12$ kG (*d*, $N = 7$, $z_{VC} = 0.7$ mm), $I_0 = 15$ kA, $B_0 = 20$ kG (*e*, $N = 1$, $z_{VC} = 2.3$ mm), $I_0 = 40$ kA, $B_0 = 20$ kG (*f*, $N = 4$, $z_{VC} = 0.9$ mm) and the side view of the beam for $I_0 = 50$ kA, $B_0 = 4$ kG (*g*, $N = 5$, $z_{VC} = 0.75$ mm); here, *1* is the cylindrical equipotential drift chamber, *2*—the entrance transparent grid electrode (the injection plane), and *3*—the cylindrical collector, Z_{VC} denotes the approximate position of the VC; the longitudinal coordinate of the cutting plane (x, y): $z_s = 2$ mm; the animated configuration portraits in the regimes *a*–*d* are shown online. Only particles behind the projection plane ($z < z_s$) are shown in the configuration portraits; arrows denote the areas of the electron bunches that are formed in the REB; and the greyscale (or color scale) denotes electrons energy. (Multimedia view) [URL: http://dx.doi.org/10.1063/1.4938216.1] [URL: http://dx.doi.org/10.1063/1.4938216.2] [URL: http://dx.doi.org/10.1063/1.4938216.3][URL: http://dx.doi.org/10.1063/1.4938216.4]

external magnetic fields. It is also known that greater the space charge density of the beam is, the closer to the injection plane is the VC formed. Consequently, the growth of the external magnetic field, leading to the increase in the space charge density (for the fixed beam current) due to the focusing, also results in the displacement of the VC to the injection plane.

V. PHYSICAL BACKGROUND FOR THE REB REGIMES SWITCHINGS

Let us investigate the physical causes which are responsible for the discovered increase in the electron bunches number in the REB with the beam current growth. To do so, let us consider the qualitative model of the rotating bunches in the REB consisting of N equal point charges $q_0(N)$ that are located symmetrically on the circle of the mean radius $R_m = R_b - d/2$. These charges are rotating with the frequency ω, and the external magnetic field B_z is applied to the model (see Fig. 6). Each charge represents the electron bunch formed in the REB in the azimuthal direction, and $q_0(N) < 0$ corresponds to the total charge of the bunch in the model with N bunches. Since all charges are identical and located symmetrically, we can analyze the motion of one arbitrary chosen charge (shown on the top of Fig. 6 schematically).

The motion of the charge bunches in the noninertial frame is determined by the action of the Lorentz, Coulomb's, and centrifugal forces, and as follows from the motion equation in cylindrical coordinates,[54] the equilibrium condition along the radial direction can be written in the following way:

$$\eta\sqrt{1-\frac{(R_m\omega)^2}{c^2}}(E_r + R_m\omega B_z) + R_m\omega^2 = 0, \tag{1}$$

where $\eta = q_0(N)/m_0(N)$ is the specific charge, $q_0(N)$ and $m_0(N)$ are the total charge and mass of the bunch, respectively, $E_r < 0$ is the radial component of the electric field intensity in the point of the arbitrary charge that can be easily determined from Coulomb's law for the considered system with $N \geq 2$ point charges as

$$E_r(N) = \frac{q_0(N)k_e}{R_m^2}\left(\sum_{i=1}^{\left[\frac{N-1}{2}\right]}\frac{\cos\dfrac{\pi(N-2i)}{2N}}{\left(1-\cos\dfrac{2\pi i}{N}\right)} + \frac{\delta(N \bmod 2)}{4}\right), \tag{2}$$

where k_e is Coulomb's constant and δ is the delta function.

Equation (1) implies that for fixed system parameters (B_z, R_m, N, and ω that are determined in the numerical simulation), there is an equilibrium total charge of an electron bunch, $q_0^{eq}(N)$, for which bunches keep a constant radius R_m in the system

$$q_0^{eq}(N) = \frac{R_m\omega}{E_r'(N)}\left(\frac{\omega}{\eta\sqrt{1-\left(\dfrac{r\omega}{c}\right)^2}} - B_z\right), \tag{3}$$

where c is the speed of light, $E_r'(N) = E_r(N)/q_0(N) > 0$.

The comparison of the equilibrium charge values for the system with N and $(N+1)$ bunches, which can be easily made with the help of Equations (3) and (2), shows that

$$\frac{q_0^{eq}(N+1)}{q_0^{eq}(N)} < 1 \tag{4}$$

i.e., the greater number of the bunches in the system, the less the charge of each bunch in the equilibrium state. In fact, the numerical simulations demonstrate a similar tendency. One can see in Fig. 7 where the dependency of the absolute value of the electron bunch mean total charge q_b on the beam current value is shown. The basic tendency, which it demonstrates, is the abrupt stepwise decrease in the charge q_b in the moments of the regime switchings and the smooth increase between the switchings because of the beam current growth. When the charge q_b approaches the critical value (when the regime switching occurs), the configuration with N bunches

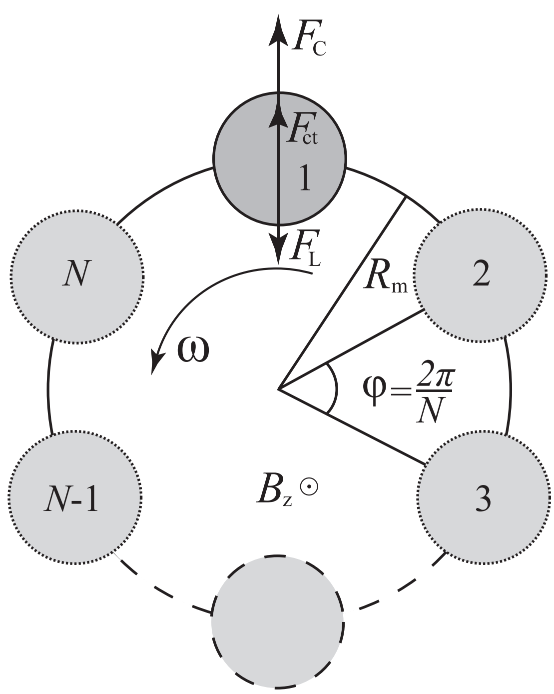

FIG. 6. The model of the rotating electron bunches at steady state. Here, R_m is the radius of the circle, N is the number of bunches, ω is the frequency of rotation, B_z is the external longitudinal magnetic field, and F_L, F_C, and F_{ct} are the Lorentz, the Coulomb's repulsion, and the centrifugal forces, respectively.

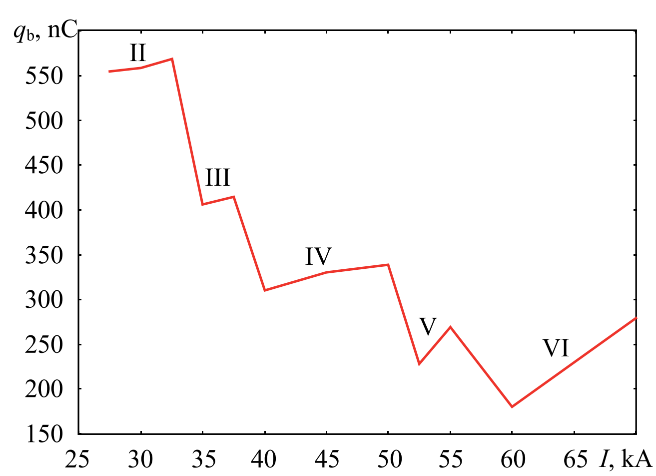

FIG. 7. The dependency of the mean total charge of electron bunch q_b on the beam current I. Roman numerals denote regimes that are realized in the system for the given beam currents; $B_0 = 18.5$ kG (see the dotted line in Fig. 4); the current step—1 kA.

becomes unstable due to space charge forces action, and finally, it leads to the establishment of the stable configuration with $N+1$ bunches with the smaller charge in each bunch.

So, the basic conclusion of the analytical treatment and numerical simulations is that the division of electron bunches with the growth of the beam current leads to the more uniform distribution of space charge in the azimuthal direction and to the formation of a new stable equilibrium configuration. While the charge of one bunch decreases after the process of the bunches division, the total charge of all bunches increases, as a consequence of the increased beam current. The obtained result also explains the switchings during the rise time of the current pulse (transient process), which, for instance, can be seen in Fig. 2. The transient time τ is substantially greater than the system's own time scale that is determined by the rotation frequency of the bunches ($\sim 20-40$ GHz). So, the transient process can be considered as "quasi-stationary," and we can extend the results of the steady-state model at each instant of time that is characterized by the certain beam current.

The physical background for the REB regimes switchings with the change in the magnetic field is similar. As a matter of fact, the growth of the magnetic field leads to the increase in the space charge density (for the fixed beam current), so when the bunch charge approaches the critical value, the configuration with N bunches is transformed to the configuration with $N+1$ bunches. But such growth of the space charge density is not so strong to cause a long sequence of the regimes switchings. At the same time, the growth of the magnetic field results in the change in the force balance due to the change of the rotation frequency. As a result, the regime map (Fig. 4) demonstrates in some cases switchings from regimes with $N+1$ bunches to regimes with N bunches with the growth of the magnetic field.

VI. CONCLUSIONS

The obtained results reveal the basic features of the development, coexistence, and interaction of Pierce-Bursian and diocotron instabilities in the nonneutral REB. It has been found out that the diocotron instability in the considered system with the tubular beam is developed due to the presence of the azimuthal velocity gradient (shear), and the bunch starts forming in the area where the azimuthal velocity changes sign from positive to negative. The physical background for the REB regimes switchings is revealed both analytically and numerically. For the first time, the important feature of the simultaneous development of the Bursian and diocotron instabilities, which the Bursian instability contributes essentially to the development of the diocotron instability, has been found out in the present work numerically. Nevertheless, this significant effect requires further more detailed studies, particularly, the formulation of the semi-analytical model of the processes of the instabilities simultaneous development.

Due to the generality of the considered model, the obtained results have additional interest because they may be extended to many systems of plasma physics and electronics where intense high-energy beams of the charged particles are used on relatively long distances or for a long time. For example, the processes occurring in the Penning trap are similar to those that are observed in the area between the injection plane and VC in the investigated system.

ACKNOWLEDGMENTS

The studies of the characteristic regimes of REB dynamics have been supported by the Russian Science Foundation (Grant No. 14-12-00222). The studies of the physical processes occurring during the development of the instabilities have been supported by the Russian Foundation for Basic Research (Nos. 15-32-20299, 14-02-00329 and 15-52-04018) and President's program (Project No. MK-5426.2015.2). The studies of physical causes being responsible for the REB regimes switchings have been supported by the Ministry of Education and Science of the Russian Federation (Project Nos. 3.59.2014/K and 931).

[1]J. Benford, J. A. Swegle, and E. Schamiloglu, *High Power Microwaves* (CRC Press; Taylor and Francis, 2007).
[2]R. E. Collin, *Foundations for Microwave Engineering*, IEEE Press Series on Electromagnetic Wave Theory, 2nd ed. (John Wiley and Sons, Inc., Hoboken, New Jersey, 2001).
[3]R. J. Barker and E. Schamiloglu, *High-Power Microwave Sources and Technologies* (IEEE Press, New York, 2001).
[4]R. J. Barker, J. H. Booske, N. C. Luhmann, and G. S. Nusinovich, *Modern Microwave and Millimeter-Wave Power Electronics* (Wiley, New York, 2005).
[5]R. C. Davidson, *Theory of Nonneutral Plasmas* (W.A. Benjamin Inc., Advanced book program, 1974).
[6]R. B. Miller, *An Introduction to the Physics of Intense Charged Particle Beams* (Plenum Press, New York, 1982).
[7]M. V. Nezlin, *Physics of Intense Beams in Plasmas,* Series in Plasma Physics (CRC Press, 1993).
[8]R. C. Davidson, *Physics of Nonneutral Plasmas* (Imperial College Press and World Scientific Publishing Co. Pte. Ltd., 2001).
[9]R. C. Davidson and H. Qin, *Physics of Intense Charged Particle Beams in High Energy Accelerators* (World Scientific Publishing Company, 2001).
[10]G. Shvets, O. Polomarov, V. Khudik, C. Siemon, and I. Kaganovich, "Nonlinear evolution of the weibel instability of relativistic electron beams," Phys. Plasmas **16**, 056303 (2009).
[11]R. A. Mahaffey, P. A. Sprangle, J. Golden, and C. A. Kapetanakos, "High-power microwaves from a non-isochronous reflecting electron system," Phys. Rev. Lett. **39**, 843 (1977).
[12]A. N. Didenko, Y. Krasik, S. P. Perelugin, and G. P. Fomenko, "Generation of power microwave radiation of relativistic beam in triode system," Tech. Phys. Lett. **5**, 321 (1979).
[13]D. J. Sullivan, J. E. Walsh, and E. A. Coutsias, *Virtual Cathode Oscillator (Vircator) Theory*, High Power Microwave Sources Vol. 13, edited by V. L. Granatstein and I. Alexeff (Artech House Microwave Library, 1987).
[14]A. E. Dubinov and V. D. Selemir, "Electronic devices with virtual cathodes (review)," J. Commun. Technol. Electron. **47**, 575 (2002).
[15]A. S. Shlapakovski, T. Queller, Y. Bliokh, and Y. E. Krasik, "Investigations of a double-gap vircator at sub-microsecond pulse durations," IEEE Trans. Plasma Sci. **40**, 1607–1617 (2012).
[16]A. E. Dubinov, I. A. Efimova, K. E. Mikheev, V. D. Selemir, and V. P. Tarakanov, "Hybrid microwave oscillators with a virtual cathode," Plasma Phys. Rep. **30**, 496 (2004).
[17]S. A. Kurkin, N. S. Frolov, A. O. Rak, A. A. Koronovskii, A. A. Kurayev, and A. E. Hramov, "High-power microwave amplifier based on overcritical relativistic electron beam without external magnetic field," Appl. Phys. Lett. **106**, 153503 (2015).
[18]J. Ju, D. Cai, G. Du, Y. Wang, L. Liu, and J. Zhang, "Characterization of cesium iodide-coated carbon-fiber aluminum cathode for an s-band high-efficiency vircator," IEEE Trans. Plasma Sci. **43**(10), 3522 (2015).

[19]V. P. Bursian and V. I. Pavlov, "About one particular case of the space charge influence on the propagation of electron beam in vacuum [in russian]," J. Russ. Phys. Chem. Soc. **55**, 71–80 (1923).
[20]J. R. Pierce, "Possible fluctuations in electron streams due to ions," J. Appl. Phys. **19**, 231 (1948).
[21]L. A. Bogdankevich and A. A. Rukhadze, "Stability of relativistic electron beams in a plasma and the problem of critical currents," Sov. Phys. Usp. **14**, 163 (1971).
[22]L. Thode, B. B. Godfrey, and W. R. Shanahan, "Vacuum propagation of solid relativistic electron beams," Phys. Fluids **22**, 747–763 (1979).
[23]A. L. Peratt and C. M. Snell, "Microwave generation from filamentation and vortex formation within magnetically confined electron beams," Phys. Rev. Lett. **54**, 1167–1170 (1985).
[24]J. A. Rome and R. J. Briggs, "Stability of sheared electron flow," Phys. Fluids **15**, 796–804 (1972).
[25]C. C. Cutler, "Instability in hollow and strip electron beams," J. Appl. Phys. **27**, 1028–1029 (1956).
[26]C. A. Kapetanakos, D. A. Hammer, C. D. Striffler, and R. C. Davidson, "Destructive instabilities in hollow intense relativistic electron beams," Phys. Rev. Lett. **30**, 1303–1306 (1973).
[27]R. L. Kyhl and H. R. Webster, "Breakup of hollow cylindrical electron beams," IRE Trans Electron Devices **3**, 172 (1956).
[28]M. A. Mostrom and M. E. Jones, "Sheardriven instabilities of annular relativistic electron beams in vacuum," Phys. Fluids **26**, 1649–1658 (1983).
[29]H. F. Webster, "Structure in magnetically confined electron beams," J. Appl. Phys. **28**, 1388–1397 (1957).
[30]Y. Carmel and J. A. Nation, "Instability of an unneutralized relativistic electron beam," Phys. Rev. Lett. **31**, 286–289 (1973).
[31]I. N. Kartashov and M. V. Kuzelev, "Nonlinear dynamics of diocotron instability," Plasma Phys. Rep. **36**, 524–532 (2010).
[32]V. V. Mikhailenko, H. J. Lee, V. S. Mikhailenko, and N. A. Azarenkov, "Non-modal analysis of the diocotron instability: Cylindrical geometry," Phys. Plasmas **20**, 042101 (2013).
[33]V. V. Mikhailenko, J. S. Kim, Y. H. Jo, V. S. Mikhailenko, and H. J. Lee, "Non-modal analysis of the diocotron instability for cylindrical geometry with conducting boundary," Phys. Plasmas **21**, 052105 (2014).
[34]S. I. Chung, H. J. Yun, S. B. Shim, M. Chung, and H. J. Lee, "Control of vortex merging induced from diocotron instability using rotating-wall electric fields," IEEE Trans. Plasma Sci. **39**, 2496–2497 (2011).
[35]J. O. Hall and P. K. Shukla, "Vortex formation in an electron plasma with a sheared flow," Phys. Plasmas **12**, 122301 (2005).
[36]B. Paroli, G. Maero, R. Pozzoli, and M. Rome, "Diocotron modulation in an electron plasma through continuous radio-frequency excitation," Phys. Plasmas **21**, 122102 (2014).
[37]D. Mikitchuk, C. Stollberg, R. Doron, E. Kroupp, Y. Maron, H. R. Strauss, A. L. Velikovich, and J. L. Giuliani, "Mitigation of instabilities in a z-pinch plasma by a preembedded axial magnetic field," IEEE Trans. Plasma Sci. **42**, 2524–2525 (2014).
[38]Y. H. Jo, V. V. Mikhailenko, V. S. Mikhailenko, and H. J. Lee, "The stabilizing effect of a conducting boundary on the diocotron instability of non-neutral electron flow," J. Korean Phys. Soc. **66**, 935–940 (2015).
[39]S. A. Kurkin, A. A. Badarin, A. A. Koronovskii, and A. E. Hramov, "Higher harmonics generation in relativistic electron beam with virtual cathode," Phys. Plasmas **21**, 093105 (2014).
[40]A. E. Hramov, S. A. Kurkin, A. A. Koronovskii, and A. E. Filatova, "Effect of self-magnetic fields on the nonlinear dynamics of relativistic electron beam with virtual cathode," Phys. Plasmas **19**, 112101 (2012).
[41]S. A. Kurkin, A. A. Koronovskii, and A. E. Hramov, "Specific features of virtual cathode formation and dynamics with allowance for the magnetic self-field of a relativistic electron beam," Plasma Phys. Rep. **39**, 296–306 (2013).
[42]S. A. Kurkin, A. E. Hramov, and A. A. Koronovskii, "Microwave radiation power of relativistic electron beam with virtual cathode in the external magnetic field," Appl. Phys. Lett. **103**, 043507 (2013).
[43]V. L. Granatstein and I. Alexeeff, *High Power Microwave Sources* (Artech House Microwave Library, 1987).
[44]S. C. Burkhart, R. D. Scarpetty, and R. L. Lundberg, "A virtual cathode reflex triode for high power microwave generation," J. Appl. Phys. **58**, 28 (1985).
[45]R. F. Hoeberling and M. V. Fazio, "Advances in virtual cathode microwave sources," IEEE Trans. Electromagn. Compat. **34**, 252–258 (1992).
[46]S. A. Kurkin and A. E. Hramov, "Virtual cathode formation in annular electron beam in an external magnetic field," Tech. Phys. Lett. **35**, 23–25 (2009).
[47]A. E. Hramov, A. A. Koronovsky, S. A. Kurkin, and I. S. Rempen, "Chaotic oscillations in electron beam with virtual cathode in external magnetic field," Int. J. Electron. **98**, 1549–1564 (2011).
[48]K. R. Clements, R. D. Curry, R. Druce, W. Carter, M. Kovac, J. Benford, and K. McDonald, "Design and operation of a dual vircator hpm source," IEEE Trans. Dielectr. Electr. Insul. **20**, 1085–1092 (2013).
[49]S. A. Kurkin, "The influence of the noise spread of electron velocities on the dynamics of an electron flow with a virtual cathode," J. Commun. Technol. Electron. **55**, 572–579 (2010).
[50]S. A. Kurkin, A. A. Koronovskii, and A. E. Hramov, "Effect of the electron beam modulation on the sub-thz generation in the vircator with the field-emission cathode," J. Plasma Phys. **81**, 1–12 (2015).
[51]E. B. Abubakirov and A. P. Konyushkov, "Peculiarities of backward-wave amplification by relativistic high-current electron beams," IEEE Trans. Plasma Sci. **38**, 1285–1291 (2010).
[52]Y. E. Krasik, A. Dunaevsky, and J. Felsteiner, "Plasma sources for high-current electron beam generation," Phys. Plasmas **8**, 2466–2472 (2001).
[53]C. K. Birdsall and A. B. Langdon, *Plasma Physics via Computer Simulation* (Taylor and Francis Group, 2005).
[54]S. E. Tsimring, *Electron Beams and Microwave Vacuum Electronics* (John Wiley and Sons, Inc., Hoboken, New Jersey, 2007).
[55]G. G. MacFarlane and H. G. Hay, "Wave propagation in a slipping stream of electrons: Small amplitude theory," Proc. Phys. Soc., Sect. B **63**, 409 (1950).
[56]R. H. Levy, "Diocotron instability in a cylindrical geometry," Phys. Fluids **8**, 1288–1295 (1965).
[57]A. J. Peurrung and J. Fajans, "Experimental dynamics of an annulus of vorticity in a pure electron plasma," Phys. Fluids A **5**, 493 (1993).
[58]R. C. Davidson and G. M. Felice, "Influence of profile shape on the diocotron instability in a non-neutral plasma column," Phys. Plasmas **5**, 3497–3511 (1998).
[59]J. Petri, "Non-linear evolution of the diocotron instability in a pulsar electrosphere: Two-dimensional particle-in-cell simulations," Astron. Astrophys. **503**, 1–12 (2009).
[60]S. Pramanik, A. Y. Ender, V. I. Kuznetsov, and N. Chakrabarti, "The transverse magnetic field effect on steady-state solutions of the bursian diode," Phys. Plasmas **22**, 042110 (2015).
[61]V. I. Kuznetsov, Y. A. Ender, H. Schamel, and P. V. Akimov, "Switching of nonneutral plasma diodes. ii. numerical results," Phys. Plasmas **11**, 3224–3233 (2004).
[62]Y. A. Ender, V. I. Kuznetsov, H. Schamel, and P. V. Akimov, "Switching of nonneutral plasma diodes. i. analytic theory," Phys. Plasmas **11**, 3212–3223 (2004).
[63]D. Biswas, "A one-dimensional basic oscillator model of the vircator," Phys. Plasmas **16**, 063104 (2009).
[64]R. A. Filatov, A. E. Hramov, Y. P. Bliokh, A. A. Koronovskii, and J. Felsteiner, "Influence of background gas ionization on oscillations in a virtual cathode with a retarding potential," Phys. Plasmas **16**, 033106 (2009).
[65]G. Singh and C. Shashank, "Particle-in-cell simulations for virtual cathode oscillator including foil ablation effects," Phys. Plasmas **18**, 063104 (2011).
[66]S. A. Kurkin, A. A. Koronovskii, and A. E. Hramov, "Output microwave radiation power of low-voltage vircator with external inhomogeneous magnetic field," Tech. Phys. Lett. **37**, 356–359 (2011).
[67]S. A. Kurkin, A. E. Hramov, and A. A. Koronovskii, "Chaotic signal generation in low-voltage vircator with electron source shielded from external magnetic field," Tech. Phys. Lett. **37**, 144–147 (2011).
[68]N. S. Phrolov, A. A. Koronovskii, Y. Kalinin, S. A. Kurkin, and A. E. Hramov, "The effect of an external signal on output microwave power of a low-voltage vircator," Phys. Lett. A **378**, 2423–2428 (2014).